Comparative study on the band structures of tetrazaporphin nickel(II) and porphyrinato nickel(II). A crystal-orbital approach based on a semiempirical Hartree-Fock self-consistent-field model

Michael C. Böhm
Max-Planck-Institut für Festkörperforschung, D-7000 Stuttgart 80, Federal Republic of Germany
(Received 5 July 1983)

The band structures of (a) tetrazaporphin nickel(II) and (b) porphyrinato nickel(II) have been studied by means of the crystal-orbital (CO) model based on the tight-binding approximation. The CO approach is performed in the self-consistent-field scheme of the Hartree-Fock formalism. The employed Hamiltonian is a semiempirical intermediate neglect of differential overlap operator that has been designed to reproduce the results of high-quality *ab initio* calculations. Interaction patterns between atomic pairs in the unit cells of the polymers and two-center combinations that belong to different layers of the one-dimensional (1D) systems have been analyzed. As a result of the pronounced charge deficit at the transition-metal centers, highly repulsive interaction energies are derived for the Ni-Ni coupling within the 1D stacks. The destabilizing metal-metal interaction is determined by classical Coulomb forces while covalent one-electron coupling and exchange effects are negligibly small. The interaction between the Ni center and pyrrole nitrogens in neighboring cells is strongly attractive due to the different net charges of the two atomic species. Both unoxidized polymers, (a) and (b), have a finite band gap; the valence and conduction bands are ligand π and π^* functions. A large number of ligand π, lone-pair, and σ bands is predicted on top of the transition-metal bands that are formed by the orbitals of the square-planar coordinated Ni centers with d^8 configuration. The closely spaced (energy criterion) ligand (π, lone-pair, σ) and transition-metal [$3d_{z^2}(\sigma)$, $3d_{xz}(\pi)$,$3d_{yz}(\pi)$, $3d_{x^2-y^2}(\delta)$] basis energies as well as the symmetry reduction D_{4h} ($\vec{k}=0$, $\vec{k}=\pi/c$)$\rightarrow C_{4v}$ ($\vec{k}\neq 0$, $\vec{k}\neq\pi/c$) for nonmarginal values of the wave vector $\vec{k}$ leads to a pronounced $\vec{k}$ dependence in the composition of the CO wave functions. Correlations between different types of ligand states ($\pi\rightarrow n$, $\pi\rightarrow\sigma$, $n\rightarrow\sigma$, etc.) and between Ni $3d$ and ligand functions are detected in the various dispersion curves. Partially oxidized modifications of (a) and (b) are organic metals with conductive pathways that are confined to the extended ligand frameworks. The computational findings are compared with available experimental results derived for recently synthesized phthalocyanine and porphyrin polymers that show unexpected physical and chemical properties in the solid state.

I. INTRODUCTION

The physical, chemical and solid-state properties of low-dimensional systems that contain transition-metal compounds with extended π ligands as molecular building blocks, have focused considerable interest in recent years.[1–3] It has been shown that face-to-face stacking of planar chelate ligands and partial oxidation due to copolymerization with halides leads to conductivities and transport properties that are comparable with the physical data that have been detected in the large class of organic metals (e.g., TTF, tetrathiafulvalene; TCNQ, tetracyanoquinodimethane).[4,5] The correspondence in the solid-state properties between the organic metals on one side and one-dimensional (1D) systems with organometallic fragments on the other side is largest in the case of phthalocyanines [system (i)] and porphyrinato stacks [system (ii)] with a large variety of transition-metal centers (see Fig. 1). Partially oxidized conducting phthalocyanine derivatives have been synthesized that contain either transition-metal atoms (Fe,Co,Ni,Cu,Zn,Pt) as central units[6,7] or that are coupled via SiO or GeO bridges.[8] A detailed investigation has been published on the solid-state, structural, spectral, and charge carrier properties of nickel(II) phthalocyanine.[9] Experimental studies in the group of porphyrinato stacks were restricted to 1D systems that contain Ni centers with d^8 configuration while convenient ligand frames are either the octamethyltetrabenzporphyrin system[10–12] or the tetrabenzo fragment.[13] The physical data of tetrabenzporphyrinato nickel(II) have been examined with the same carefulness as those of nickel(II) phthalocyanine.[13]

On the other hand, less is known about the electronic structures of these molecular metals in the solid state. Lattice stabilization energies in phthalocyanine derivatives have been determined semiquantitatively by means of Haber-Born circles.[14] Such procedures however give no insight into the nature of the electron states of the polymer, into the sequence of the metal $3d$ and ligand functions and into the transport properties of the low-dimensional compounds. The suitable theoretical framework for an investigation of the latter quantities is the crystal-orbital (CO) formalism that has been derived in the tight-binding approximation.[15,16] The band-structure

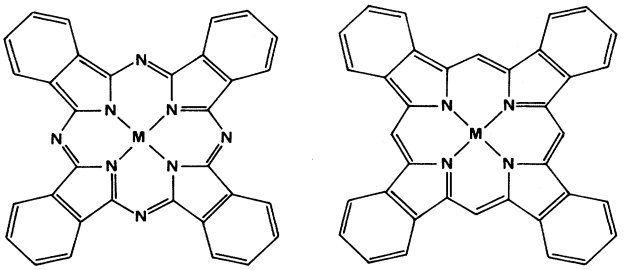

(i) (ii)

FIG. 1. Phthalocyanine system (i) and tetrabenzporphyrinato system (ii). *M* symbolizes a transition-metal center (e.g., Fe,Co,Ni,Cu,Zn,Pt) or a SiO-GeO bridge [in system (i)].

technique in combination with the self-consistent-field (SCF) equations based on the Hartree-Fock (HF) ansatz has become a powerful and important tool to study the solid-state properties of polymers with small and medium-sized unit cells and atom combinations of the first row.[17,18] The large unit-cell dimensions encountered in phthalocyanines and porphyrins of course prevent the application of CO variants that are based on *ab initio* Hamiltonians. The sparse tight-binding calculations on transition-metal stacks with extended organic ligands therefore were restricted to simple one-electron operators based on the Wolfsberg-Helmholtz (WH) or extended Hückel (EH) approximation.[19,20] The classical contributions of Mott[21,22] and Slater[23] as well as recent theoretical studies of Whangbo[24,25] on the other side have shown that models with one-electron Hamiltonians (e.g., WH or EH operators) are not suitable tools for studying the band-structure properties of 1D systems with transition-metal units as the magnitude of the electron-electron interaction determines whether a polymer or a solid is an insulator, a semiconductor, or a conductor.

To render CO calculations on the stage of the HF SCF approximation in the case of transition-metal stacks with macrocyclic ligands we have developed a crystal-orbital model that is based on a semiempirical CNDO-INDO Hamiltonian (CNDO, complete neglect of differential overlap; INDO, intermediate neglect of differential overlap).[26] The ZDO (zero differential overlap)[27] operator has been parametrized to reproduce the results of extended basis set *ab initio* calculations in molecules and one-dimensional chains in the framework of an effective all-valence Hamiltonian.[28] The method has been used successfully to elucidate the band structures and the solid-state properties of transition-metal polymers with medium-sized and larger ligand moieties [e.g., nickel(II) glyoximates,[29,30] polyferrocenylene,[31] bis(glyoximato)-pyrazine iron,[32] bis(benzoquinonedioximato)nickel(II)[33]]. In these contributions we have studied geometrical preferences in the solid state, the physical nature of metal-metal, metal-ligand, and ligand-ligand interactions within the unit cells of the 1D ensembles and the two-center coupling between atomic sides that belong to different molecular fragments. Furthermore, we have analyzed the band-structure properties (relative ordering of metal and ligand bands), the density-of-states distribution and the conductive pathways in partially oxidized modifications of the transition-metal stacks.

In this paper we want to extend our theoretical CO studies to suitable model chains for nickel(II) phthalocyanine and tetrabenzporphyrinato nickel(II) as the unit-cell dimensions of both stacks are too large, even for HF SCF CO variants that are derived by means of semiempirical Hamiltonians based on the ZDO approximation. The model systems employed in the present study are displayed in Fig. 2. A suitable model unit for the phthalocyanine skeleton is tetrazaporphin nickel(II) [system (iii)] while porphyrinato nickel(II) [system (iv)] has been adopted as representative example in the porphyrinato family where tetrabenzo derivatives have focused most of the experimental interest in recent years. Preliminary results on the band structures of systems (iii) and (iv) as derived by the INDO variant of the present ZDO CO formalism have been reported in previous contributions.[34,35]

Computational details of the semiempirical INDO HF SCF CO calculations (e.g., lattice sum dimensions, number of $\vec{k}$ points employed in the determination of the bands, damping techniques) are mentioned in the next paragraph. The band-structure properties of systems (iii) and (iv) as well as interaction patterns between neighboring unit cells are analyzed in the following section.

II. COMPUTATIONAL ASPECTS

The physical background, the basis equations,[15,16] and the theoretical shortcomings[36] of the crystal orbital formalism have been described in large detail in the literature and are thus not reviewed in this contribution. The present INDO CO model has been discussed in Ref. 26. A review on the sparse solid-state approaches to 1D systems with transition-metal atoms can be found in Ref. 37 (e.g., CO formalism, augmented-plane-wave, and orthogonalized-plane-wave calculations).

The HF SCF technique in the tight-binding approximation leads to a set of coupled complex Hermitian pseudoeigenvalue problems that must be solved point by point in reciprocal $\vec{k}$ space where $\vec{k}$ is a convenient wave vector

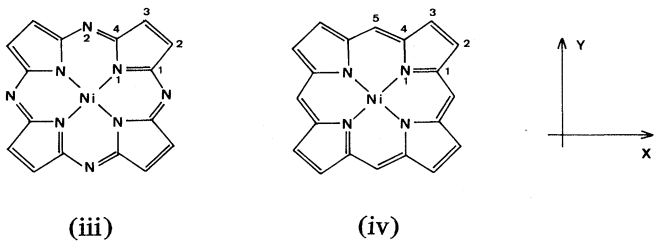

(iii) (iv)

FIG. 2. Tetrazaporphin nickel(II) system (iii) and porphyrinato nickel(II) system (iv). The atomic numbering scheme used in the text and the tables is displayed in the drawings. The employed coordinate system is shown on the right side; the stacking axis lies in the *z* direction.

associated to the translational symmetry in the infinite system; the chain is characterized due to periodic Born—von Karman boundary conditions. The HF SCF CO equations are coupled via the charge-density bond-order matrices that are calculated by means of numerical integration over the $\vec{k}$ vector within the first Brillouin zone. In the case of system (iv) we have solved the HF SCF CO equations in the framework of an accelerated Hartree damping of the charge-density bond-order matrices.[38] This simple method failed in the CO calculations on system (iii) with its additional heteroatoms. With decreasing damping parameters in the course of the SCF iterations shell swapping between the occupied and virtual Fermi seas had always been encountered. To avoid these difficulties we combined the accelerated Hartree damping at the beginning of the iterative procedure with the direct steepest descent method of McWeeny[39] that has been inserted after the first five SCF steps controlled by the damping algorithm. The direct energy minimization via a steepest descent formalism has been employed in previous semiempirical CO calculations on 1D systems with closely spaced filled and empty Fermi seas and ill-conditioned trial orbitals where the convenient matrix diagonalizations were unsuccessful.[40] The Hartree damping in the first SCF steps is a necessary condition in the computational approach as roundoff errors prevented keeping the idempotency of the charge-density bond-order matrices. The central processing unit times for the INDO CO calculations on system (iii) and (iv) amount to 6—8 h on an IBM 370/168 computer.

To get some insight into the physical nature of metal-metal and metal-ligand coupling within the reference cell and between neighboring unit cells, we have decomposed the total energy of the polymer (normalized to one unit cell), E_{tot}, into intracell (E_{intra}) and intercell (E^j_{inter}) contributions where j symbolizes the jth neighboring unit cell ($j=1,2,\ldots,$ reference cell $j=0$). In the case of ZDO models it is always possible to decompose E^j_{inter} into diatomic interaction energies E^{AB}_s. Two-center potentials can be extracted also from the net intracell energy.[27] The total two-center energy is divisible into the so-called resonance term (E^{AB}_{res}), which is determined by the kinetic energy (one-electron operator) of the electrons that belong to the atoms A and B, into an exchange element E^{AB}_{ex} due to the antisymmetry of the determinantal wave function in the HF approximation and into the classical electrostatic interaction energy E^{AB}_{Cou} which is the sum of electron-electron, electron-core, and core-core interactions. The necessary formulas for the determination of E^{AB}_{res}, E^{AB}_{ex}, and E^{AB}_{Cou}, respectively, have been derived in our previous contribution.[26] The magnitude of the three terms allows a classification of the various interaction patterns (intracell versus intercell) in the 1D strand and leads to quantitative insight into the relative importance of the two-electron part of the Hamiltonian in comparison to the covalent coupling which is determined by the resonance energy E^{AB}_{res} (one-electron operator).

Our previous CO studies on transition-metal stacks have shown that at least five neighbors (index j) should be taken into account in the evaluation of the lattice sums.[28,33] Smaller j arrays cause significant errors both in the band positions and in the width of the dispersion curves; the charge distribution depends less on the number of neighbors considered in the lattice sum. The INDO CO results for systems (iii) and (iv) thus have been derived in the fifth neighbor's approximation. The $\vec{k}$-dependent eigenvalue problems have been solved at ten points in reciprocal $\vec{k}$ space. The iterative SCF procedures on systems (iii) and (iv) have been continued until the energy differences between two subsequent steps are less than 10^{-4} a.u.

In order to allow a critical valuation and classification of the INDO CO data, the following points must be mentioned.

(i) The neglect of electron correlation in the Hartree-Fock approximation leads to calculated band gaps between the occupied and empty Fermi seas that are too large in comparison to experimental data. This difference (theory versus experiment) is diminished in the case of effective Hamiltonians where experimental two-electron integrals are employed in the various formulas. Dressed electron-electron parameters cause a renormalization of the two-electron part of the Hamiltonian and a renormalization of the filled and unfilled one-particle spaces.[41] Two-electron quantities that are close to experimental parameters are used in the present INDO CO variant.[26,28]

(ii) Renormalized electron-electron interaction integrals reduce furthermore the failures of the HF approximation to describe the virtual one-particle space by means of a $V_{(N-1)}$ potential instead of the convenient V_N potential (N number of electrons per unit cell) encountered in the HF formalism.[42,43] The calculated INDO CO gaps based on an effective Hamiltonian thus should be a reliable approximation to true band gaps.

(iii) It is well known that the ZDO approximation in band-structure calculations leads to values for the band width that are systematically too broad in the filled subspace of the crystal orbitals, but that are too narrow in the empty subspace.[44—46] These effects are negligibly small in the extreme outer valence region (highest filled and lowest empty bands), they are enhanced with increasing (decreasing) energies for the dispersion curves of occupied (virtual) bands.

(iv) It is still a contested question whether or not resonance integrals in ZDO-based model calculations on systems with weakly coupled extended fragments are properly determined by means of the convenient approximations adopted in semiempirical ZDO procedures[47,48]; previous theoretical approaches favor computational methods for the one-electron interaction that correspond to an orthogonalized atomic orbital (AO) basis. The combined effects mentioned under (iii) and the AO basis problem suggest that the width of the energy bands should be slightly overestimated in the present crystal orbital study.

The density of states $N(E)$ of the systems (iii) and (iv) have been calculated by means of a classical definition[49,50]; the $N(E)$ histograms were constructed by means of a discrete summation over N_k $\vec{k}$ points ($N_k=50\,000$). The dispersion curves were approximated via fourth-order polynomials that have been determined in a least-squares

TABLE I. Decomposition of the total energy E_{tot}, of the polymers system (iii) [tetrazaporphin nickel(II)] and system (iv) [porphyrinato nickel(II)] into intracell contributions, E_{intra}, and into intercell energies E^j_{int} between the reference cell and the jth neighboring cell encountered in the lattice sum according to the semiempirical INDO CO formalism. E^j_{inter} is the total intercell energy calculated in the fifth-nearest-neighbor approximation. All values in eV.

Polymer system	E_{intra}	E^1_{inter}	E^2_{inter}	E^3_{inter}	E^4_{inter}	E^5_{inter}	E^j_{inter}	E_{tot}
(iii)	−4971.5370	−6.1420	−0.4136	−0.2707	−0.2025	−0.1616	−7.1904	−4978.7274
(iv)	−4736.7895	−5.4793	−0.4360	−0.2808	−0.2084	−0.1654	−6.5699	−4743.3594

fit to the ten available $\vec{k}$ points.

We have adopted the geometrical parameters of Refs. 9 and 13 for the CO calculations on the model polymers systems (iii) and (iv). Both sets of x-ray data correspond to partially oxidized nickel(II) phthalocyanine and porphyrinato nickel(II) polymers where the Ni centers crystallize in a face-to-face arrangement while the π planes of the organic ligands are perpendicular to the stacking axis. The unit-cell dimensions c employed in the present study amount to 3.244 Å [system (iii)] and 3.217 Å [system (iv)], respectively. The molecular frames in the Ni phthalocyanine and tetrabenzporphyrinato derivatives are staggered by an angle of about 40° between neighboring unit cells. INDO CO calculations on the rotational profile of system (iv) however have shown that the eclipsed 0° orientation corresponds to the energy minimum in the smaller porphyrinato stack.[51] Therefore, we have studied the band structures of systems (iii) and (iv) only for the 0° orientation where the maximum D_{4h} symmetry is conserved only at the center of the Brillouin zone (Γ point) and at the edge of the zone (X point). The symmetry of the crystal orbitals is reduced to C_{4v} at all other points in reciprocal $\vec{k}$ space.

The following bond lengths have been accepted in the case of systems (iii) and (iv). System (iii): NiN_1 (pyrrole nitrogen), 1.887 Å; $N_1C_1=N_1C_4$, 1.379 Å; C_1N_2(azamethine nitrogen)$=C_4N_2$, 1.320 Å; C_2C_3, 1.392 Å; $C_1C_2=C_3C_4$, 1.456 Å. System (iv): NiN_1, 1.966 Å; $N_1C_1=N_1C_4$, 1.401 Å; $C_1C_5=C_4C_5$, 1.340 Å; C_2C_3, 1.392 Å, $C_1C_2=C_3C_4$, 1.443 Å. A common standard parameter of 1.1 Å has been adopted for the various C—H bonds.[52]

III. RESULTS AND DISCUSSION

An energy fragmentation for the 1D systems (iii) and (iv) into intracell and intercell contributions is summarized in Table I. The total intercell energy E^j_{inter} calculated in the fifth-nearest-neighbor approximation amounts to about −7.20 eV [system (iii)] and to −6.57 eV [system (iv)], respectively. These coupling elements between the different layers in the two stacks are only ~0.14% of the total (intracell and intercell) energy of the polymers. The nearest-neighbor coupling contributes more than 80% to E^j_{inter}. The E^j_{inter} numbers of systems (iii) and (iv) differ by ~0.63 eV. This distinction in the intercell energy must be traced back to the magnitude of E^1_{inter}, the coupling element between the reference cell and the nearest neighbor. The E^1_{inter} contribution calculated for the tetrazaporphin stack system (iii) exceeds the corresponding parameter in the 1D system (iv) significantly.

The global decomposition into net intercell energies however prevents the understanding of individual two-center coupling patterns within the molecular building blocks and between atoms in different unit cells of the low-dimensional systems. In order to rationalize the physical nature of important two-center interactions we have divided some diatomic interaction potentials into the aforementioned elements E^{AB}_{res}, E^{AB}_{ex}, and E^{AB}_{Cou}. To simplify the theoretical analysis we have calculated the atomic net charges q_i in the unit cells of systems (iii) and (iv). The q_i numbers[53] are summarized in Table II. It is seen that the transition-metal centers in both polymers have a pronounced charge deficit which is almost comparable in the two systems. Important differences in the charge distribution however are encountered in the macrocyclic ligand moieties. A stronger polarization of the electronic charge is diagnosed in the 1D system (iii) with eight heteroatoms per unit cell. The largest charge shift is found between the pyrrole nitrogens on one side (charge excess, −0.7889) and the adjacent carbon centers C_1 and C_4 on the other side; a deficit of 0.6025 is predicted at these ligand atoms. The topologically related q_i separation in the porphyrinato polymer system (iv) is less pronouced. The q_i numbers for N_1 and $C_1=C_4$ amount to −0.6731 and 0.3811. The charge excess at the azamethine nitrogens in system (iii) is less marked in comparison to the electron distribution at the four pyrrole centers. The difference between both types of heteroatoms of course must be traced back to the combined effects of intraligand polarization and metal-to-ligand charge transfer at the pyrrole N atoms while the latter transfer

TABLE II. Atomic net charges of tetrazaporphin nickel(II) (iii) and porphyrinato nickel(II) (iv) according to the semiempirical INDO CO formalism in the fifth-nearest-neighbor approximation. The atomic numbering scheme is explained in Fig. 2.

Atom	System (iii)	System (iv)
Ni	1.1824	1.1769
N_1	−0.7889	−0.6731
$C_1=C_4$	0.6025	0.3811
$C_2=C_3$	−0.2160	−0.1972
N_2[system (iii)], C_5[system (iv)]	−0.5829	−0.3973
$H_2=H_3$	0.1516	0.1305
H_5[system (iv)]		0.1474

TABLE III. Energy fragmentation for the two-center potentials between the Ni centers in systems (iii) and (iv) and for the NiN_1 interaction between atoms in different unit cells. The intracell energy between the Ni atom and the pyrrole nitrogens is also summarized. The two-center interaction energies in the INDO CO formalism are separated into resonance (E^{AB}_{res}), exchange (E^{AB}_{ex}), and classical electrostatic (E^{AB}_{Cou}) contributions; E^{AB}_{Cou} is the sum of electron-electron, electron-core, and core-core interaction. The intercell energies have been decomposed as a function of the j neighboring unit cell considered in the lattice sum. $E^{AB}_s = E^{AB}_{res} + E^{AB}_{ex} + E^{AB}_{Cou}$. All values in eV.

Polymer system	Two-center pair (intercell)	Coupling element	Interaction energy with the jth cell $j=1$	$j=2$	$j=3$	$j=4$	$j=5$	Net interaction $j=1-5$
(iii)	NiNi	E^{AB}_{res}	−0.0546	−0.0005				−0.0551
		E^{AB}_{ex}	−0.0276	−0.0134	−0.0090	−0.0067	−0.0054	−0.0621
		E^{AB}_{Cou}	3.0302	1.5418	1.0312	0.7743	0.6197	6.9972
		E^{AB}_s	2.9480	1.5279	1.0222	0.7675	0.6143	6.8799
	NiN_1	E^{AB}_{res}	−0.1039	−0.0001				−0.1040
		E^{AB}_{ex}	−0.0037	−0.0002	−0.0001	−0.0001	−0.0001	−0.0042
		E^{AB}_{Cou}	−1.7373	−0.9847	−0.6745	−0.5108	−0.4106	−4.3179
		E^{AB}_s	−1.8449	−0.9848	−0.6746	−0.5109	−0.4107	−4.4261
(iv)	NiNi	E^{AB}_{res}	−0.0529	−0.0006				−0.0535
		E^{AB}_{ex}	−0.0276	−0.0135	−0.0090	−0.0068	−0.0054	−0.0623
		E^{AB}_{Cou}	3.0264	1.5408	1.0306	0.7738	0.6194	6.9910
		E^{AB}_s	2.9460	1.5283	1.0215	0.7670	0.6140	6.8752
	NiN_1	E^{AB}_{res}	−0.1007	−0.0001				−0.1008
		E^{AB}_{ex}	−0.0036	−0.0002	−0.0001	−0.0001		−0.0040
		E^{AB}_{Cou}	−1.4691	−0.8399	−0.5766	−0.4370	−0.3514	−3.6740
		E^{AB}_s	−1.5734	−0.8401	−0.5767	−0.4371	−0.3514	−3.7788

Polymer system	Two-center pair (intracell)	E^{AB}_{res}	E^{AB}_{ex}	E^{AB}_{Cou}	E^{AB}_s
(iii)	NiN_1	−4.3843	−0.8468	−6.4968	−11.7278
(iv)	NiN_1	−4.0210	−0.8078	−5.3372	−10.1661

mechanism is not active at the azamethine sides. A remarkable surplus of electronic charge is calculated also at the carbon center C_5 in the porphyrinato nickel(II) system (iv). The estimated net charges in the central CC moieties C_2C_3 of the pyrrole ring are comparable in both metallamacrocycles.

The calculated q_i numbers allow a straightforward explanation of the results of the energy fragmentation summarized in Table III. The two-center energy for the Ni—N bonds within the molecular frames of systems (iii) and (iv) are divided into resonance, exchange, and electrostatic interaction elements (bottom of Table III); this decomposition is also given for the metal-metal interaction in the 1D stacks as well as for the coupling between the transition-metal center in the reference cell and the pyrrole nitrogens (N_1) in the neighboring layers. The Ni-Ni and Ni-N_1 potentials have been separated into contributions from the different unit cells taken into account in the lattice sums.

The intracell energies (Ni-N pairs) exceed −10 eV. The leading terms to E^{AB}_s are the classical electrostatic energies, the sums of electron-electron repulsion, electron-core attraction, and the destabilization of the atomic cores; E^{AB}_{Cou} contributes more than 50% to E^{AB}_s.

The interaction pattern predicted for the transition-metal—ligand bonds differs significantly from the E^{AB}_s composition (magnitude of $E^{AB}_{res}, E^{AB}_{ex}, E^{AB}_{Cou}$) of typical ligand-ligand bonds in the organic π system where more than 65% of the two-center energy are determined by the covalent one-electron interaction. This difference in the E^{AB}_s figures is of course one of the sources of the remarkable success of the electrostatic ligand-field theory[54] in electronic structure theory of transition-metal compounds.

The coupling elements for the two different intercell pairs are once again modified in comparison to the interaction terms within the molecular units. The pronounced charge deficit at the Ni centers leads to highly repulsive Coulomb energies between the transition-metal atoms in the 1D stacks; the electrostatic interaction parameters between adjacent Ni sides are larger than 3 eV in both polymers. These destabilizing E^{AB}_{Cou} terms are added to nearly 7 eV in the fifth-nearest-neighbor approximation. This computational result (repulsive Ni-Ni coupling and vanishing "covalent" contribution in the metal-metal interaction) differs from the suggestions of previous qualitative and semiquantitative models that have been published in the case of polynuclear and infinite transition-metal systems with face-to-face stacking of the metal

atoms. Stabilizing interaction energies have been postulated for the mutual metal-metal coupling.[2,55,56]

The highly charged nature of the transition-metal atoms on the contrary is responsible for the strongly repulsive Ni-Ni contributions to the total energies of the polymers. It is our opinion that the results summarized in Table III [repulsive Ni-Ni potentials in systems (iii) and (iv)] are not an artifact of the Hartree-Fock approximation where electron correlation is neglected although an adequate theoretical description of the electronic structure in weakly coupled transition complexes is only possible by means of large-scale CI (configuration interaction) expansions[57–59]; calculated correlation energies (for neutral polyatomic model clusters) on the other side are small in comparison to the electrostatic contributions that have been diagnosed for the Ni-Ni coupling in systems (iii) and (iv).

Important stabilizing diatomic intercell potentials are predicted for the interaction between the positivated transition-metal atom in the reference cells and the pyrrole nitrogens in the neighboring fragments which have a pronounced charge excess. Larger two-center energies (NiN_1) are encountered in the tetrazaporphin system (iii) where a stronger charge accumulation at N_1 [in comparison to system (iv)] has been calculated. The stabilizing E_s^{AB} (A=Ni, B=N_1) elements for the nearest-neighbor interaction amount to -1.84 eV in system (iii) and to -1.57 eV in the porphyrinato system (iv). The most important terms in the E_s^{AB} numbers are once again the classical electrostatic interaction energies. The different intercell energies in systems (iii) and (iv) (Table I) can be traced back (at least in part) to the distinction in the E_s^{AB} values for the NiN_1 pairs where the two atoms belong to different layers in the polymers. The total energy E_s^{AB} between the central atom and the pyrrole N sides is summarized to -4.43 eV in the tetraza stack while a value of -3.38 eV per NiN_1 pair is derived for the model chain (iv) (fifth-neighbor approximation).

The energy fragmentation in the case of the Ni-Ni pairs and NiN_1 ensembles has shown that face-to-face stacking in the solid state of macrocyclic organometallics is not a consequence of stabilizing interactions between the transition-metal centers; this contribution to E_{tot} is in any case highly repulsive. The metal-over-metal arrangement in the 1D systems however allows an efficient magnification of stabilizing interaction terms between the 3d center in the reference cell and the pyrrole nitrogens in the neighboring ligand moieties. Deviations from the *M-M* (metal-metal) crystallization are obviously accompanied by a reduction of the electrostatic interaction energy between the two types of atoms with opposite net charges (Ni and N_1).

The largest net contributions to the lattice sums nevertheless are resonance and exchange terms while the sum of the various diatomic electrostatic interaction energies is much smaller. The remarkable individual E_{Cou}^{AB} terms nearly compensate each other due to a comparable number of stabilizing and destabilizing Coulomb contributions. The charge excess in the ligand framework, e.g., leads to a magnification of repulsive E_{Cou}^{AB} pairs that reduce the stabilizing intercell Coulomb energies that have been discussed for the diatomic interactions in the central molecular spheres (Ni atoms, pyrrole centers) of the macrocyclic ligands.

TABLE IV. Wiberg bond indices of tetrazaporphin nickel(II) (iii) and porphyrinato nickel(II) (iv) in the framework of the INDO CO approach. The atomic numbering scheme is explained in Fig. 2.

Bond	System (iii)	System (iv)
NiN_1	0.2562	0.2521
$N_1C_1=N_1C_4$	1.1527	1.1849
$C_1C_2=C_3C_4$	1.1069	1.1261
C_2C_3	1.7116	1.7115
$C_1N_2=C_4N_2$[system (iii)]	1.3371	
$C_1C_5=C_4C_5$[system (iv)]		1.3822
$C_2H_2=C_3H_3$	0.9677	0.9720
C_5H_5[system (iv)]		0.9647

The Wiberg bond indices[60] collected in Table IV are a rough measure for the strength of the metal-ligand and ligand-ligand bonds (intracell) in systems (iii) and (iv). The metal-ligand interaction is comparable in both transition-metal compounds; this is also true for the central C—C bonds in the five-membered rings. Differences are observed for the heterobonds $N_1C_1=N_1C_4$ and the C—C bonds $C_1C_2=C_3C_4$. Both types of ligand atoms are more strongly coupled to the porphyrinato system (iv) while the enhanced charge separation at the corresponding centers in system (iii) leads to a decrease of the ligand-ligand interaction.

The density of states $N(E)$ histograms for all filled valence bands (both unoxidized polymers have a finite band gap) of systems (iii) and (iv) are displayed in Fig. 3.

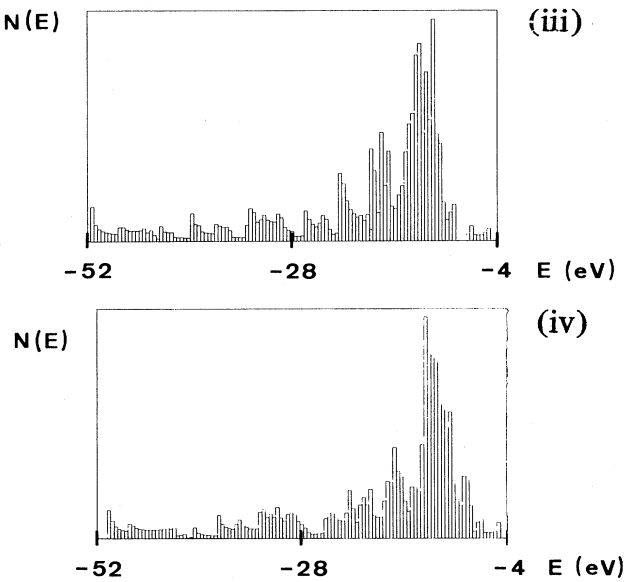

FIG. 3. Density-of-states histograms for all filled valence bands of tetrazaporphin nickel(II) (ii) and porphyrinato nickel(II) (iv) according to the semiempirical INDO CO formalism. The energy grid employed in the $N(E)$ diagrams amounts to 0.4 eV. A common scale factor has been used to normalize the height of the $N(E)$ peaks.

The energy grid employed in the $N(E)$ histograms amounts to 0.4 eV. The two $N(E)$ plots are quite similar in the region below -20 eV. The density-of-states distribution of system (iii) shows an energy gap in the extreme outer valence region (-9.25 to -7.24 eV) while strongly overlapping bands in system (iv) lead to an $N(E)$ profile without any gaps. Larger differences in the $N(E)$ distributions of systems (iii) and (iv) are found in the outer valence region above -20 eV. The highest peak maxima in the $N(E)$ plot of the tetrazaporphin stack are predicted in an interval between -13.7 and -11.4 eV. The range of high $N(E)$ peaks is smaller in the porphyrinato derivative system (iv) (-13.6 to -12.4 eV). The electropositive CH fragments in system (iv) [in comparison to the azamethine N functions of system (iii)] cause higher peaks on the low-energy side of the aforementioned $N(E)$ maxima; a dramatic $N(E)$ reduction in the region above -11.4 eV on the other side is encountered in the tetraza stack system (iii).

The dispersion curves and the associated density-of-states distributions for filled and empty bands of systems (iii) and (iv) in the interesting region between -20 and 0 eV are displayed in Figs. 4 and 5; the energy width in the density of states diagrams is 0.25 eV. The forbidden band gap in system (iii) is calculated to be 1.56 eV, while a value of 2.01 eV is derived for the porphyrinato polymer. Both results are in line with experimental studies on nickel(II) phthalocyanine and on various porphyrinato nickel(II) derivatives which are all insulators in the absence of oxidants.[9,13] The room-temperature conductivity of the nickel phthalocyanine stack, e.g., is 1×10^{-11} $(\Omega\,\mathrm{cm})^{-1}$ and the activation energy for the conductivity is 1.6 eV.

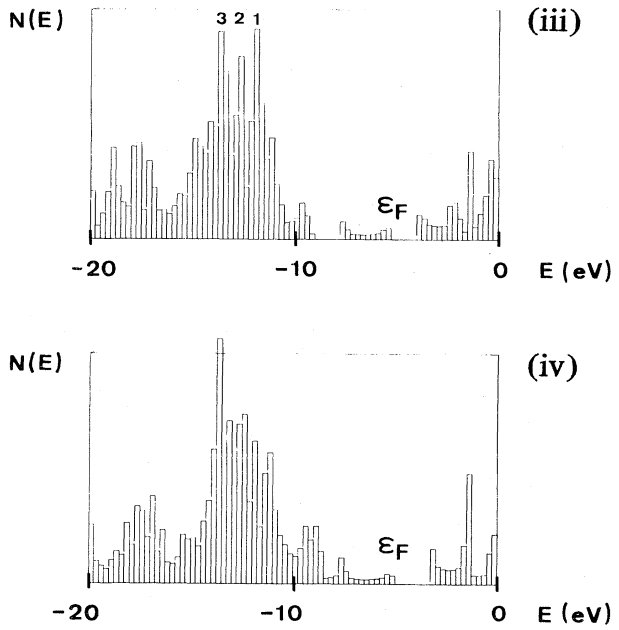

FIG. 5. Density-of-states distribution for the filled and unfilled bands of tetrazaporphin nickel(II) (iii) and porphyrinato nickel(II) (iv) in the region between -20 and 0 eV; the associated $\epsilon(k)$ curves are displayed in Fig. 4. The energy grid employed in the $N(E)$ diagrams amounts to 0.25 eV. A common scale factor has been adopted for the normalization of the peaks in the $N(E)$ plot. ϵ_F symbolizes the Fermi level for the unoxidized stacks systems (iii) and (iv). The peak maxima (1,2,3) in the upper diagram are explained in the text.

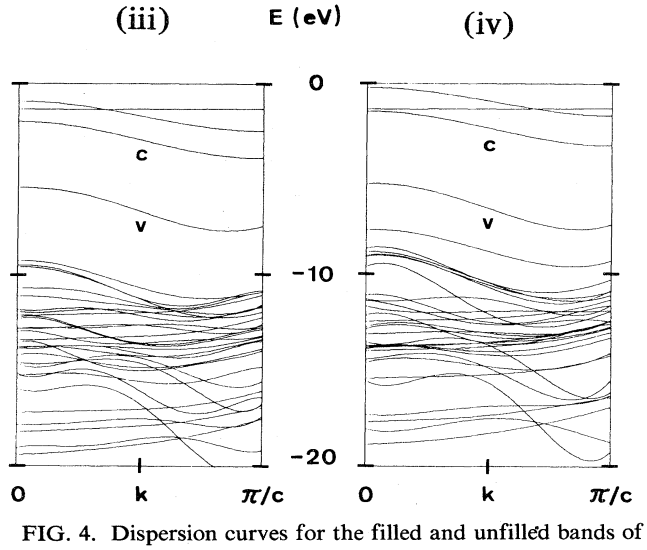

FIG. 4. Dispersion curves for the filled and unfilled bands of tetrazaporphin nickel(II) (iii) and porphyrinato nickel(II) (iv) in the region between -20 and 0 eV according to the semiempirical INDO CO approach. v symbolizes the valence bands of the unoxidized polymers and c stands for the conduction bands. The valence bands in both systems are of ligand π character (a_2 symmetry with the labels of C_{4v}), the degenerate conduction bands are ligand π^* functions (e symmetry, C_{4v}).

The valence bands of the unoxidized polymers (iii) and (iv) are ligand π functions, and are of a_2 symmetry if the irreducible representations of C_{4v} are employed. The degenerate conduction bands are also associated to the ligand frameworks (π^*,e symmetry). The two bands (valence and conduction bands) are related to the molecular orbitals (MO's) $a_{1u}(\pi)$ and $e_g(\pi^*)$ (irreducible representations correspond to the point group D_{4h}). Theoretical and spectroscopic studies on phthalocyanine and porphyrinato complexes have shown that these MO's are the highest occupied (a_{1u}) and lowest virtual (e_g) one-electron functions in the molecular building units.[61,62] The frontier orbital sequence is thus not modified in the energy bands encountered in the solid state. The lowest strong absorptions in nickel phthalocyanine at 693 and 621 nm have been assigned as ligand centered $\pi\rightarrow\pi^*$ transitions ($a_{1u}\rightarrow e_g$ in the case of D_{4h} symmetry labels).[9] This assignment is corroborated by means of the INDO CO data (valence and conduction bands) derived for system (iii).

The $\epsilon(k)$ curves for the highest filled and lowest empty bands of systems (iii) and (iv) show an opposite dispersion; the top of the bands is predicted at the zone center while the bottom is found at the edge of the Brillouin zone. Opposite $\epsilon(k)$ curves in the extreme outer valence region have been observed in different CO approaches on organic 1D stacks with extended π ligands.[63,64] It is easy to explain these unexpected dispersions encountered in chains with

macrocyclic π fragments as the molecular building blocks. A schematic representation of the CO amplitudes of the valence and conduction bands of system (iii) is displayed in Fig. 6; both crystal orbital wave functions have a large number of nodes. The Γ states in the bands are given by in-phase combinations of the CO wave functions between the different cells, the X states on the other side are characterized by out-of-phase interactions between topologically identical atoms in the unit cells of the polymer. The large number of nodes in the wave functions of the outer valence bands leads to an overcompensation of the intercell interactions between equal atomic sides; the band energies are lowered with increasing values of the $\vec{k}$ vector. A staggered orientation between the molecular fragments in the 1D chains lifts this opposite $\epsilon(k)$ dispersion.[51]

The calculated band width $\Delta\epsilon$ for the valence and conduction bands of system (iii) amount to 2.24 and 1.88 eV, respectively. The two $\Delta\epsilon$ numbers in the porphyrinato system are similar to the tetrazaporphin values; $\Delta\epsilon$ parameters of 2.34 and 1.77 eV are observed in the framework of the semiempirical INDO CO formalism. The theoretically determined values for the width of the valence bands in systems (iii) and (iv) differ remarkably from experimental estimates that have been derived on the basis of magnetic susceptibility measurements on partially oxidized phthalocyanine and porphyrin stacks (injected holes). The "experimental" width has been extrapolated by means of simple formulas where the Pauli susceptibility of a degenerate electron gas is related to a single one-electron matrix element for the intercell interaction.[9,13] The estimated $\Delta\epsilon_{\text{val}}$ parameters of systems (iii) and (iv) amount to $\sim$0.4 eV. The difference between theory and experimentally deduced numbers on one side must be traced back to the fact that electron correlation, which leads to a narrowing of the $\epsilon(k)$ curves, is neglected in a crystal orbital approach on the stage of the HF level. On the other side it is clear that the employed formulas for the extrapolation of $\Delta\epsilon_{\text{val}}$ are only very rough approximations derived on the basis of a simplified Hubbard Hamiltonian. We have used the term "valence band" as the aforementioned experiments correspond to partially oxidized stacks with injected holes.

The character of the filled bands of systems (iii) and (iv) that are predicted below the valence bands depend strongly on the value of the $\vec{k}$ vector. The closely spaced basis energies [ligand π, ligand n (lone-pair), ligand σ, Ni $3d_{z^2}, 3d_{xz}, 3d_{yz}, 3d_{x^2-y^2}$ as σ, π, and δ functions in a square-planar arrangement] and the symmetry reduction from D_{4h} at the marginal Γ and X points to C_{4v} for $\vec{k}$ values that differ from 0 or π/c allow the formation of energy band where the CO amplitudes differ dramatically at the top and the bottom of the various $\epsilon(k)$ curves. Mutual interconversions in the character of the CO wave function in typical ligand bands are summarized below:

$$\pi \leftrightarrow n \ ,$$

$$\pi \leftrightarrow \sigma \ ,$$

$$n \leftrightarrow \sigma \ .$$

In the case of system (iii) further degrees of freedom are available as two topologically different types of nitrogen lone-pair functions are encountered in this transition-metal system, azamethine lone-pair orbitals n_a as well as pyrrole lone-pair functions n_p. An additional $\vec{k}$-dependent intraligand variation of the CO wave function, for example, is the correlation of n_a states with n_p-type CO's in an energy band. Furthermore, avoided crossings between transition-metal bands ($3d_{z^2}$, $3d_{xz}$, $3d_{yz}$, $3d_{x^2-y^2}$) and ligand bands in reciprocal $\vec{k}$ space must be taken into account; the associated $\epsilon(k)$ values belong to dispersion curves with CO's that are strongly localized at the 3D centers (ligands) at the Γ point while the wave function is of ligand (transition-metal) character at the edge of the Brillouin zone. These aspects have been discussed in some detail in a previous study.[33]

The second-highest filled band (no. 60) of system (iii) is of ligand π character at the Γ point, the states at the bottom of the band (opposite dispersion) are strongly localized azamethine lone-pair functions. The same behavior is predicted for the degenerate band 58/59. The character of the CO wave functions is conserved in the (following) bands 57 (b_2 symmetry) and 56 (a_1) which are of ligand π type both at the center and the edge of the Brillouin zone.

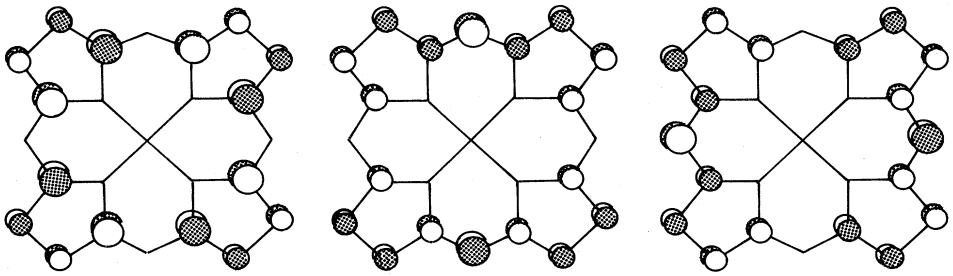

FIG. 6. Crystal orbital amplitudes in the valence (v,61) and the degenerate conduction (c,62/63) bands of the tetrazaporphin nickel(II) (iii). The simplified representation is valid both at the center and the edge of the Brillouin zone; the $\vec{k}$ dependence of the CO wave functions is rather weak.

Strongly $\vec{k}$-dependent CO amplitudes are predicted in the degenerate band 54/55 where the Γ states are ligand π orbitals while the X states are pyrrole lone-pair functions. Opposite localization properties are found in the band between -11.80 ($k=0$) and -11.66 eV ($k=\pi/c$); the states at the zone center are azamethine lone-pair functions which are transferred into ligand π amplitudes at the edge of the zone. The $\vec{k}$ dependence of the CO wave function in the a_1 band 51 is displayed in Fig. 7. n_a states at the Γ point correlate with Ni $3d_{z^2}/n_p$ functions at the edge of the zone. The first pronounced maximum in the $N(E)$ histogram of system (iii) (Fig. 5) has its origin in the $\epsilon(k)$ curves of the latter n_a lone-pair states in the vicinity of the zone center where the dispersion is very weak. The second maximum in the $N(E)$ diagram (-12.7 eV) must be traced back to energy bands that correspond to pyrrole lone-pair combinations that are coupled with the Ni $3d_{z^2}$AO of the transition-metal center. High-lying ligand σ bands lead to the last intense peak in the $N(E)$ plot of system (iii). Bands with pronounced Ni $3d$ amplitudes are predicted at still lower energies.

Dispersion curves with large Ni $3d$ admixtures are labeled in the $\epsilon(k)$ plot displayed in Fig. 8. The relative ordering of the Ni $3d$ states is $3d_{z^2} > 3d_{x^2-y^2} > 3d_{xz}/3d_{yz}$ ($\sigma > \delta > \pi$) both at the zone center and the edge of the Brillouin zone. It is seen however in Fig. 8 that the transition-metal character is not conserved as a function of the $\vec{k}$ vector. The $3d_{z^2}$ states at the Γ point correlate with ligand π functions, while the Ni $3d\delta$ and $3d\pi$ states are converted into ligand σ functions if $\vec{k}$ is increased. The Ni $3d$ functions at the edge of the zone are derived from azamethine lone-pair ($3d_{z^2}$), ligand π ($3d_{x^2-y^2}$), as well as π and σ ($3d_{xz}/3d_{yz}$) states which are predicted at the center of the zone in the aforementioned bands.

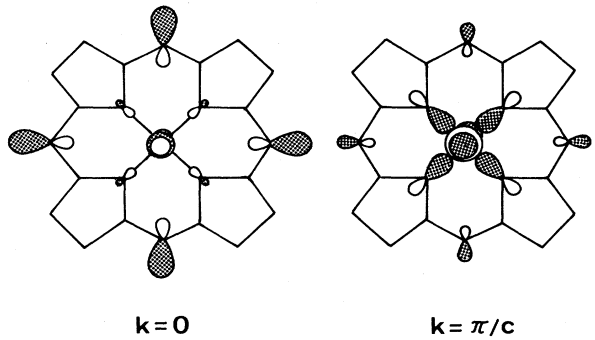

FIG. 7. Crystal orbital amplitudes at the zone center ($k=0$) and the zone edge ($k=\pi/c$) of band 51 in the tetrazaporphin nickel(II) system (iii) according to the INDO CO approach. The Γ states are prevailingly of azamethine lone-pair character, the X states are the out-of-phase combination of $3d_{z^2}$ functions with pyrrole lone-pair orbitals.

The sequence of the energy bands (ordering of high-lying ligand states and Ni $3d$ states) in system (iv) is closely related to the filling scheme predicted for the tetrazaporphin chain system (iii). The $\epsilon(k)$ curves below the valence band [nos. 60 (a_1), 58/59 (e), 57 (b_2), 56 (a_1), 54/55 (e), 53 (b_1), 52 (b_2), and 50/51 (e)] are all of ligand π character at the center of the Brillouin zone. The type of CO wave function is conserved in the bands

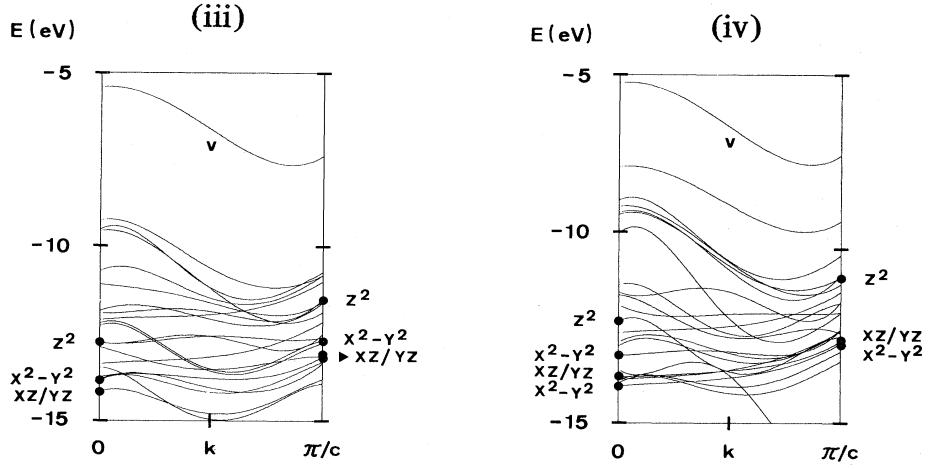

FIG. 8. Dispersion curves for the filled bands of the tetrazaporphin nickel(II) system (iii) and the porphyrinato nickel(II) system (iv) in the outer valence region between -15 and -5 eV. Bands with significant Ni $3d$ admixtures at the marginal $\vec{k}$ points are labeled in the $\epsilon(k)$ plots. The following abbreviations are used for the Ni $3d$ orbitals: $z^2=3d_{z^2}$, $x^2-y^2=3d_{x^2-y^2}$, $xz=3d_{xz}$, $yz=3d_{yz}$. The Ni $3d$ admixtures to the CO's of system (iii) at the Γ point amount to 62.7% (z^2), 95.3% (x^2-y^2), and 81.7% (xz/yz); the corresponding numbers at the zone edge are 57.4% (z^2), 94.6% (x^2-y^2), 40.2% and 38.6% (xz/yz). In the case of the porphyrinato system the following Ni $3d$ contributions are predicted at the center of the Brillouin zone: 44.0% (z^2), 43.7% (x^2-y^2), 95.6% (xz/yz) and 36.4% (x^2-y^2). The calculated Ni $3d$ amplitudes at the X point are 40.6% (z^2), 90.4% (xz/yz), and 69.1% (x^2-y^2). Only those bands are labeled where the Ni $3d$ character exceeds 35%. v symbolizes the valence bands of systems (iii) and (iv).

60,57,54/55 but is modified in the case of the remaining dispersion curves. The characters of the CO wave functions at the Γ and X points in these bands of the Ni(II) system (iii) are summarized below (L symbolizes the porphyrinato ligand):

band	character of the CO wave function	
	Γ point	X point
58/59	$L(\pi)$	$L(n)$
56	$L(\pi)$	$L(n)$, Ni $3d_{z^2}$
53	$L(\pi)$	$L(\sigma)$, Ni $3d_{z^2}$
52	$L(\pi)$	$L(n)$
50/51	$L(\pi)$	$L(\sigma)$

Significant pyrrole lone-pair admixtures are predicted in the neighborhood of the zone center in the bands below dispersion curve 50/51. Various high-lying σ ribbon orbitals are found on top of the dispersion curves with large Ni $3d$ contributions. The "Ni $3d$ bands" of system (iv) are also shown in Fig. 8 (remarkable transition-metal amplitudes at the marginal $\vec{k}$ points Γ and X). The sequence of the Ni $3d$ states at the center of the Brillouin zone is comparable with the Ni $3d$ splitting pattern in system (iii); the Ni $3d\sigma$ ($3d_{z^2}$) states are predicted on top of Ni $3d\pi$— and Ni $3d\delta$—type CO's. A switch between the $3d\pi$ and $3d\delta$ states is predicted at the X point. The $\epsilon(k)$ curves in Fig. 8 indicate that the character of the CO wave functions is not conserved in the case of the Ni $3d_{z^2}$ and $3d_{x^2-y^2}$ states if the $\vec{k}$ vector is enlarged. The Ni $3d_{z^2}$ functions at $k=0$ correlate with σ ribbon orbitals of the extended organic ligand at the edge of the zone (see Fig. 9); the same behavior is found for the Ni functions of δ symmetry. On the other hand, a degenerate Ni $3d\pi$ band (42/43) is predicted that is strongly localized at the transition-metal center (>90%) for all $\vec{k}$ values in the first Brillouin zone. The weak dispersion of the associated $\epsilon(k)$ curve leads to the pronounced $N(E)$ maximum in the density-of-states plot of system (iv) at −13.7 eV (Fig. 5). The remaining maxima on the low-energy side of this peak are due to the dispersion curves of pyrrole lone-pair and ligand σ bands.

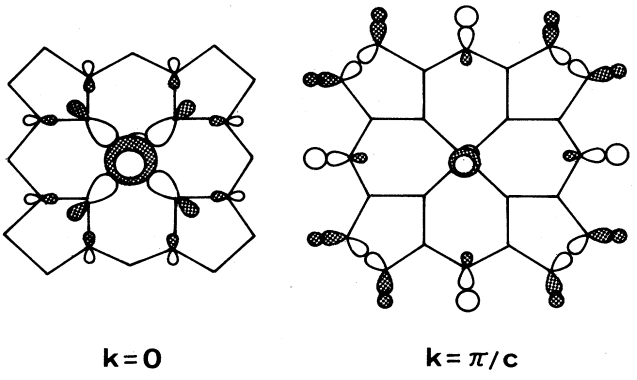

FIG. 9. Schematic representation of the CO amplitudes of band 43 in the porphyrinato nickel(II) system (iv) at the center of the Brillouin zone ($k=0$) and at the zone edge ($k=\pi/c$). The Γ states are the out-of-phase combination of Ni $3d_{z^2}$ (44%) and pyrrole lone-pair functions, the states at the X point are of ligand σ character (C—C and C—H bonds).

The Ni $3d$ states of systems (iii) and (iv) at the zone center are predicted in the following intervals: −12.79 to −14.16 eV [system (iii)] and −12.10 to −13.94 eV [system (iv)]. The center of gravity (Γ point) in both polymers differs by ~0.5 eV. The $\epsilon(k=\pi/c)$ values for Ni $3d\sigma$, $3d\pi$, and $3d\delta$ are between −11.54 to −13.18 eV [system (iii)] and −10.82 to −12.68 eV [system (iv)].

The calculated sequence of the metal and ligand states in the two unoxidized 1D systems is closely related to the results of *ab initio* and semiempirical INDO calculations on a large number of molecular transition-metal complexes with Ni centers in a d^8 configuration.[65–70] The highest occupied ligand orbitals are always predicted above the Ni $3d$ set. This ordering is quite independent from the coordination pattern and from the type of the organic π ligands; typical examples where ligand MO's are found above the Ni $3d$ functions are bis(π-allyl) (Refs. 65 and 66) and bis(π-pentadienyl) (Ref. 67) complexes with one or two Ni centers, planar bis(phenylenediamino)nickel(II) (Ref. 68), and thiochelate complexes with square-planar π ligands.[69,70]

If the INDO CO results that have been derived for the unoxidized transition-metal stacks (iii) and (iv) are transferred to oxidized polymer modifications with partially filled bands, the effects of electron relaxation and correlation within the Ni $3d$ regime must be roughly estimated in the computational approach. It is of course impossible to determine these energies quantitatively in one-dimensional systems with unit-cell dimensions as encountered in systems (iii) and (iv). On the other hand, it is a straightforward procedure to extrapolate basic quantum-mechanical results on the magnitude and importance of electronic reorganization from simpler transition-metal systems to the tetrazaporphin nickel(II) and porphyrinato nickel(II) stacks. A large number of theoretical studies in different degrees of sophistication have been published in recent years where electron correlation and relaxation in mononuclear and weakly coupled polynuclear transition-metal compounds are analyzed in large detail; the close correspondence between molecular and solid-state phenomena has been pointed out by Whangbo.[24]

Semiempirical INDO calculations[71] as well as large basis set *ab initio* studies[72–75] on cationic transition-metal hole states in weakly coupled $3d$ complexes have shown that the symmetry adapted HF solutions are unstable. The energy is significantly lowered if the spatial point symmetry is violated yielding hole states that are localized at a single transition-metal center. This hole localization corresponds to a self-reorganization of the $(N-1)$ electron system from the physically inadequate delocalized description to the proper localized valence-band structure; the correlation type that leads to this symmetry breaking is interatomic left-right correlation. This behavior supports the suggestion that also the "exact" wave function is characterized due to spatially broken symmetries, i.e., the hole localization is not an artifact due to the limitations of the HF approximation. The reliability of broken symme-

try solutions versus symmetry-adapted wave functions in binuclear transition-metal complexes has been studied recently in some detail.[76] The experimental evidence for localized hole states in various polynuclear transition-metal complexes has been demonstrated by means of various spectroscopic investigations (Mössbauer, electron spectroscopy for chemical analysis, ir, uv, EPR).[77,78] Theoretical techniques in $3d$ complexes pointing towards the possibility of symmetry breaking have been reported in different contributions[79–82]; the computational approaches are based on the investigation of the Thouless instability conditions.[83] The solid-state counterparts of the aforementioned hole localization in polynuclear $3d$ complexes are solutions of the charge-density wave and spin-density wave type that are either commensurate or incommensurate with the lattice depending on the degree of oxidation in the $3d$ regime.

The energy fragmentation for the Ni-Ni interaction (Table III) shows impressively (magnitude of the one-electron resonance interaction versus the two-electron coupling, compare with the definition of the g parameter of McLachlan and Ball[84]) that superstructures in the $3d$ regimes of systems (iii) and (iv) must be expected which, in the simplest case, cause a doubling of the unit cell and a bisection of the Brillouin zone in $\vec{k}$ space. One of the possible consequences of this instability is the trapping of localized hole states (polaron trapping),[85] the carrier transport in the metal spine is then some kind of excitonic hopping.

The second type of electronic reorganization in the $3d$ regimes in partially oxidized modifications of systems (iii) and (iv) is the strongly localized (intra-atomic) relaxation which is always accompanied by the variation of the pair correlation in the cationic hole states as many-body response.[86,87] These local rearrangement processes are quite independent from the type of the organic ligands; in the first place they are a function of the transition-metal center and its oxidation state as well as of the geometry of the complex. The reorganization elements (relaxation and correlation) for localized Ni hole states with d^7 configuration (netural parent, d^8) amount to 2.7—3.0 eV in the computational framework of the present effective INDO Hamiltonian.[70,87] The hypothetical Fermi levels ϵ_F for injected holes in the transition-metal spines of systems (iii) and (iv) are therefore found in an interval between -9.1 [system (iii)] and -7.9 [system (iv)]; these values are in any case the upper limits for ϵ_F parameters that correspond to localized Ni $3d$ hole states in the transition-metal chains. Both estimated Fermi levels are far from the ϵ_F energies for ligand centered oxidation processes which, for example, are encountered in the region between -5.46 and -7.62 eV for partially oxidized modifications of the tetrazaporphin nickel(II) stack. The ϵ_F elements are associated to experimentally available stoichiometries of $NiPcI_x$, $0 \leq x \leq 3.81$, that have been synthesized in nickel phthalocyanine (NiPc) derivatives with iodine as oxidant.[9] Fermi levels (ligand states) for incomplete charge transfer derivatives of system (iv) are found in a comparable energy range.

The combination of the INDO CO band energies determined for unoxidized modifications of the 1D stacks (iii) and (iv) with (molecular) reorganization corrections derived for square-planar Ni d^8 systems allow an extrapolation from the neutral polymers to oxidation states in the solid state that contain injected holes. The theoretical approach suggests that conducting modifications of both low-dimensional systems are organic metals with charge carriers that are localized in the macrocyclic ligands. This prediction is in line with the results of single-crystal electron spin resonance studies in $NiPcI_{1.0}$ where it has been shown that the iodine oxidation is exclusively ligand centered; the phthalocyanine moieties are organic π radical cations.[9] The same behavior (e.g., charge carriers in the ligand framework) has been verified in the case of octamethyltetrabenzporphyrinato nickel(II) (Ref. 11) which is one of the synthetically accessible derivatives in the family of highly conducting porphyrinato nickel(II) compounds. The associated idealized model system is the 1D stack (iv). The EPR data in tetrabenzoporphyrinato nickel(II) however are of larger complexity.[13] The measured carrier spin g values and linewidths led to the conclusion that the 1D stack exhibits a doubly mixed valence state with oxidation processes that are both ligand ($> 80\%$) and metal ($< 20\%$) centered.

IV. CONCLUSION

The band structures of tetrazaporphin nickel(II) and porphyrinato nickel(II) have been studied by means of crystal orbital calculations that are based on a semiempirical INDO Hamiltonian. An analysis of the interaction pattern between the transition-metal centers in the 1D stacks has shown that the Ni-Ni coupling is highly repulsive; the diatomic interaction potential is exclusively determined by Coulomb forces while covalent one-electron resonance contributions are negligibly small. This coupling mechanism suggests that the mean-field (HF) description breaks down in the (hypothetical) case of partially filled "Ni $3d$ bands" where the formation of a superstructure relative to the lattice with $c \simeq 3.2$ Å must be expected that lowers the energy of the 1D system

The INDO CO results however have shown that conducting tetrazaporphin and porphyrinato nickel(II) systems belong to the class of organic metals with ligand centered oxidation processes. An investigation of the band structures of systems (iii) and (iv) displayed that the type of the CO wave function in the energy bands depends critically on the value of the wave vector $\vec{k}$. Transformations of CO amplitudes in the ligand subspace (π/n, π/σ, n/σ, etc.) are found on one side. Additionally CO variations have been detected in various outer valence bands that embrace both Ni $3d$ and ligand states. The necessary condition for this $\vec{k}$-dependent interaction is the dense manifold of different ligand (π,n,σ) and Ni $3d$ ($3d_{z^2}$, $3d_{xz}$, $3d_{yz}$, $3d_{x^2-y^2}$) basis energies as well as the symmetry reduction $D_{4h} \rightarrow C_{4v}$ for nonmarginal values of the $\vec{k}$ vec-

tor. The $\epsilon(k)$ diagrams are characterized by a large number of avoided crossings of the dipsersion curves. This strong $\vec{k}$ dependence in the composition of the CO wave function is a typical solid-state effect that is found in 1D ensembles with extremely large unit cells.

ACKNOWLEDGMENTS

This work has been supported by the Stiftung Volkswagenwerk. The author wants to express his thanks to Professor P. Fulde for stimulating discussions and his critical reading of the manuscript.

[1]*Low Dimensional Cooperative Phenomena,* edited by H. J. Keller (Plenum, New York, 1975); *Chemistry and Physics of One Dimensional Metals,* edited by H. J. Keller (Plenum, New York, 1978); H. J. Keller, in *Mixed Valence Compounds,* edited by H. B. Brown (Reidel, Dordrecht, 1980), p. 387.

[2]*Molecular Metals,* edited by W. A. Hatfield (Plenum, New York, 1979); M. Hanack, Nachr. Chem. Techn. Lab. 8, 632 (1980); M. Hanack and G. Pawlowski, Naturwissenschaften 69, 266 (1982).

[3]J. A. Ibers, L. J. Pace, J. Martinsen, and B. M. Hoffman, *Structure and Bonding* (Springer, Berlin, 1982), Vol. 50, p. 1.

[4]Z. G. Soos, Annu. Rev. Phys. Chem. 25, 121 (1974); Z. G. Soos and D. J. Klein, in *Molecular Association,* edited by R. Foster (Academic, New York, 1975).

[5]*Physics and Chemistry of Low-Dimensional Solids,* edited by L. Alcazar (Plenum, New York, 1980); J. J. André, A. Bieber, and F. Gautier, Ann. Phys. (Paris) 1, 145 (1976); J. B. Torrance, Acc. Chem. Res. 12, 79 (1979).

[6]J. L. Petersen, C. S. Schramm, D. R. Stojakovic, B. M. Hoffman, and T. J. Marks, J. Am. Chem. Soc. 99, 286 (1977).

[7]C. J. Schramm, D. R. Stojakovic, B. M. Hoffman, and T. J. Marks, Science 200, 47 (1978).

[8]K. F. Schoch, B. R. Kundalkar, and T. J. Marks, J. Am. Chem. Soc. 101, 7071 (1979); T. J. Marks, K. F. Schoch, and B. R. Kundalkar, Synth. Met. 1, 337 (1980).

[9]C. J. Schramm, R. P. Scaringe, D. R. Stojakovic, B. M. Hoffman, J. A. Ibers, and T. J. Marks, J. Am. Chem. Soc. 102, 6702 (1980).

[10]T. E. Phillips and B. M. Hoffman, J. Am. Chem. Soc. 99, 7734 (1977).

[11]T. E. Phillips, R. P. Scaringe, B. M. Hoffman, and J. A. Ibers, J. Am. Chem. Soc. 102, 3435 (1980).

[12]B. M. Hoffman, T. E. Philipps, and Z. G. Soos, Solid State Commun. 33, 51 (1980).

[13]J. Martinsen, L. J. Pace, T. E. Phillips, B. M. Hoffman, and J. A. Ibers, J. Am. Chem. Soc. 104, 83 (1982).

[14]W. B. Euler, M. E. Melton, and B. M. Hoffman, J. Am. Chem. Soc. 104, 5966 (1982).

[15]T. E. Peacock and R. McWeeney, Proc. Phys. Soc. London 74, 385 (1959).

[16]G. del Re, J. Ladik, and G. Biczo, Phys. Rev. 155, 997 (1967); J. M. André, L. Gouverneur, and G. Leroy, Int. J. Quantum Chem. 1, 451 (1967).

[17]M. Kertesz, J. Koller, and A. Azman, *Recent Advances in the Quantum Theory of Polymers,* Vol. 113 of *Lecture Notes in Physics* (Springer, Berlin, 1980), p. 56.

[18]J. Ladik and S. Suhai, in *Molecular Interactions,* edited by W. J. Orville-Thomas and H. Ratajczak (Wiley, New York, 1980), p. 151; in *Theoretical Chemistry,* edited by C. Thomson (Royal Society of Chemistry, London, 1981), Vol. 4, p. 49.

[19]F. F. Seelig, Z. Naturforsch. Teil A 34, 986 (1979).

[20]F. F. Seelig, Mol. Cryst. Liq. Cryst. 81, 285 (1982); F. F. Seelig, Z. Naturforsch. Teil A 37, 1158 (1982).

[21]N. F. Mott, Proc. Phys. Soc. London, Sect. A 62, 416 (1949); I. G. Austin and N. F. Mott, Science 168, 71 (1970).

[22]N. F. Mott, *Metal-Insulator Transitions* (Taylor and Francis, London, 1974).

[23]J. C. Slater, Phys. Rev. 82, 538 (1951).

[24]M.-H. Whangbo, J. Chem. Phys. 70, 4963 (1979); 73, 3854 (1980).

[25]M.-H. Whangbo, M. L. Foshee, and R. Hoffmann, Inorg. Chem. 19, 1723 (1980).

[26]M. C. Böhm, Theor. Chim. Acta 62, 351 (1983).

[27]J. A. Pople and D. L. Beveridge, *Approximate Molecular Orbital Theory* (McGraw-Hill, New York, 1970).

[28]M. C. Böhm and R. Gleiter, Theor. Chim. Acta 59, 127 (1981); 59, 153 (1981).

[29]M. C. Böhn, Theor. Chim. Acta 62, 373 (1983).

[30]M. C. Böhm, Z. Phys. Chem. (Neue Folge) 133, 25 (1983).

[31]M. C. Böhm, Phys. Lett. 93A, 205 (1983).

[32]M. C. Böhm, Chem. Phys. 76, 1 (1983).

[33]M. C. Böhm, J. Phys. C 16, 1631 (1983).

[34]M. C. Böhm, Phys. Lett. 94A, 371 (1983).

[35]M. C. Böhm, Solid State Commun. 45, 117 (1983).

[36]J. C. Slater, *Quantum Theory of Molecules and Solids* (McGraw-Hill, New York, 1974), Vol. 4.

[37]D. W. Bullett, in *Solid State Physics,* edited by H. Ehrenreich, F. Seitz, and D. Turnbull (Academic, New York, 1980), Vol. 35.

[38]D. R. Hartree, *The Calculation of Atomic Structure* (Wiley, New York, 1957).

[39]R. McWeeny, Proc. R. Soc. London Ser. A 235, 496 (1956).

[40]A. Imamura and H. Fujita, J. Chem. Phys. 61, 115 (1974).

[41]H. Gutfreund and W. A. Little, Phys. Rev. 183, 68 (1969); B. H. Brandow, Int. J. Quantum Chem. 15, 207 (1979).

[42]H. P. Kelly, Phys. Rev. 131, 690 (1963); Adv. Chem. Phys. 14, 129 (1969).

[43]W. Hunt and W. A. Goddard III, Chem. Phys. Lett. 3, 414 (1969).

[44]J. L. Bredas, R. R. Chance, R. Silbey, G. Nicolas, and P. Durand, J. Chem. Phys. 75, 255 (1981).

[45]A. Karpfen, J. Chem. Phys. 75, 238 (1981).

[46]P. G. Perkins, A. K. Marwaha, and J. J. P. Stewart, Theor. Chim. Acta 57, 1 (1980).

[47]J. Koutecký and J. Paldus, in *Modern Quantum Chemistry, Instanbul Lectures, Part III,* edited by O. Sinanoğlu (Academic, New York, 1965), p. 229.

[48]J. Spanget-Larsen, Theor. Chim. Acta 55, 165 (1980); H. Vogler, *ibid.* 60, 65 (1981).

[49]J. Delhalle, in *Electronic Structure of Polymers and Molecular Crystals,* edited by J. M. André and J. Ladik (Plenum, New York, 1975). p. 53.

[50]J. Brust, *Methods in Computational Physics* (Academic, New York, 1968), Vol. 8.

[51]M. C. Böhm, Int. J. Quantum Chem. (in press).

[52]*Tables of Interatomic Distances and Configuration in Molecules and Ions,* edited by L. E. Sutton (The Chemical Society, London, 1965).

[53]R. S. Mulliken, J. Chem. Phys. 23, 1833 (1955).
[54]C. J. Ballhausen, *Introduction to Ligand Field Theory* (McGraw-Hill, New York, 1962); J. S. Griffith, *The Theory of Transition Metal Ions* (Cambridge University Press, Cambridge, 1971).
[55]S. M. Peng, J. A. Ibers, and R. H. Holm, J. Am. Chem. Soc. 98, 8037 (1978); S. M. Peng and V. L. Goedken, *ibid.* 98, 8500 (1976).
[56]H. Endres, H. J. Keller, R. Lehmann, A. Poveda, H. H. Rupp, and H. van de Sand, Z. Naturforsch. Teil B 32, 516 (1977).
[57]I. Shim, J. P. Dahl, and H. Johansen, Int. J. Quantum Chem. 15, 311 (1979); I. Shim, Theor. Chim. Acta 54, 113 (1980).
[58]M. M. Goodgame and W. A. Goddard, J. Chem. Phys. 85, 215 (1981).
[59]P. M. Atha, I. H. Hillier, and M. F. Guest, Chem. Phys. Lett. 75, 84 (1980); P. M. Atha and I. H. Hillier, Mol. Phys. 45, 285 (1982).
[60]K. B. Wiberg, Tetrahedron 24, 1083 (1968).
[61]M. C. Zerner and M. Gouterman, Theor. Chim. Acta 4, 44 (1966); A. M. Schaffer, M. Gouterman, and E. R. Davidson, *ibid.* 30, 9 (1973).
[62]M. Gouterman, G. H. Wagnière, and L. C. Snyder, J. Molec. Spectrosc. 11, 108 (1963); L. Edwards and M. Gouterman, *ibid.* 33, 292 (1970).
[63]R. D. Singh and J. Ladik, Phys. Lett. 65A, 264 (1978).
[64]S. Suhai and J. Ladik, Phys. Lett. 77A, 25 (1980).
[65]A. Veillard, J. C. S. Chem. Commun. 1967, 1022; 1967, 1427; M.-M. Rohmer and A. Veillard, *ibid.* 1973, 250; M.-M. Rohmer, J. Demuynck, and A. Veillard, Theor. Chim. Acta 36, 93 (1974).
[66]M. C. Böhm, R. Gleiter, and C. D. Batich, Helv. Chim. Acta 63, 990 (1980); M. C. Böhm and R. Gleiter, Theor. Chim. Acta 57, 315 (1980).
[67]M. C. Böhm and R. Gleiter, Chem. Phys. 64, 183 (1982); M. C. Böhm, Ber. Bunsenges, Phys. Chem. 86, 56 (1982); Theor. Chim. Acta 60, 455 (1982).
[68]J. Weber, C. Daul, A. v. Zelewsky, A. Goursot, and E. Penigault, Chem. Phys. Lett. 88, 78 (1982).
[69]Z. S. Herman, R. F. Kirchner, G. H. Loew, U. T. Mueller-Westerhoff, A. Nazzal, and M. C. Zerner, Inorg. Chem. 21, 46 (1982).
[70]M. C. Böhm, Z. Phys. Chem. (Neue Folge) 129, 149 (1982).
[71]M. C. Böhm, R. Gleiter, F. Delgado-Pena, and D. O. Cowan, Inorg. Chem. 19, 1081 (1980); J. Chem. Phys. 79, 1154 (1983).
[72]H. van Dam, D. J. Stufkens, A. Oskam, M. Doran, and I. H. Hillier, J. Electron Spectrosc. 21, 47 (1980); H. van Dam, J. N. Louwen, A. Oskam, M. Doran, and I. H. Hillier, *ibid.* 21, 57 (1980).
[73]P. A. Cox, M. Benard, and A. Veillard, Chem. Phys. Lett. 87, 159 (1982); M. Benard and A. Veillard, *ibid.* 90, 160 (1982); M. Benard, Theor. Chim. Acta 61, 379 (1982).
[74]R. P. Messmer, T. C. Caves, and C. M. Kao, Chem. Phys. Lett. 90, 296 (1982).
[75]M. D. Newton, Chem. Phys. Lett. 90, 291 (1982).
[76]M. Benard, Chem. Phys. Lett. 96, 183 (1983).
[77]D. O. Cowan, C. LaVenda, J. Park, and F. Kaufman, Acc. Chem. Res. 9, 207 (1973).
[78]N. S. Hush, in *Mixed-Valence Compounds,* edited by D. B. Brown (Reidel, Dordrecht, 1980), p. 151; T. J. Meyer, in *Mixed-Valence Compounds,* edited by D. B. Brown (Reidel, Dordrecht, 1980), p. 75; P. N. Schatz, in *Mixed-Valence Compounds,* edited by D. B. Brown (Reidel, Dordrecht, 1980), p. 115.
[79]M. C. Böhm, Ber. Bunsenges. Phys. Chem. 85, 755 (1981); Theor. Chim. Acta 60, 233 (1981).
[80]M. C. Böhm, Mol. Phys. 46, 255 (1982).
[81]M. C. Böhm, Int. J. Quantum Chem. 24, 185 (1983).
[82]M. Benard, J. Chem. Phys. 71, 2546 (1979).
[83]D. J. Thouless, Nucl. Phys. 21, 255 (1960); *The Quantum Mechanics of Many-Body Systems* (Academic, New York, 1961).
[84]A. D. McLachlan and M. A. Ball, Rev. Mod. Phys. 36, 844 (1964).
[85]T. Holstein, Ann. Phys. 8, 343 (1959).
[86]M. C. Böhm, Theor. Chim. Acta 61, 539 (1982).
[87]M. C. Böhm, J. Chem. Phys. 78, 7044 (1983).